Holy Water: Photo-Brightening in Quasi-2D Perovskite Films under Ambient Enables Highly Performing Light-Emitting Diodes

Yanyan Duan, Freddy E. Oropeza, Xueze Jin, Olivia Amargós-Reyes, Youssef Atoini, Luca M. Cavinato, Gergely Norbert Nagy, Mousumi Upadhyay Kahaly, Víctor A. de la Peña O'Shea, De-Yi Wang, and Rubén D. Costa*

Quasi-2D perovskites provide new opportunities for lighting and display applications due to their high radiative recombination and excellent stability. However, seldom attention has been placed on their self-stability/working operation under ambient storage. Herein, quasi-2D perovskites/Polyethylene oxide (PEO) films are studied, showing an unforeseen photo-brightening effect under ambient storage (i.e., an increase of the photoluminescence quantum yield from 55% to 74% after 100 days). In stark contrast, those stored under a dark/inert atmosphere show a significant decrease down to 38%. This counterintuitive phenomenon responds to the increasing radiative recombination rate caused by the passivation of the surface Br vacancies in the presence of physically adsorbed water molecules, as corroborated by in situ/ex situ X-ray photoelectron spectroscopy and density functional theory calculations. Capitalizing on this surprising effect, stable light-emitting diodes (LEDs) using quasi-2D perovskites/PEO color filters are fabricated, realizing high stabilities of ≈400 h@10 mA under operating ambient conditions, representing a 20-fold enhancement compared to LEDs with 3D counter partners. Hence, this study reveals a unique insight into the impact of water passivation on the optical/structural properties of quasi-2D perovskite films, broadening their applications under operating ambient conditions.

1. Introduction

Recently, solution-processed metal halide perovskites (MHPs) have attracted a significant attention in the lighting field.[1–5]

Their excellent optical properties, like high photoluminescence quantum yields (PLQYs), narrow emission band, color tunability by controlling the composition, low material cost, mild synthetic temperature (<100 °C) stand out over other conventional organic emitters – e.g., Ir(ppy)$_3$ or the inorganic CdSe/ZnS quantum dots (QDs)[6–10] for both, color down-converting filters in light-emitting diodes (LEDs)[11,12] and electroluminescent materials in thin-film devices.[13] Unfortunately, the stability of the MHPs under ambient conditions still remains as the biggest obstacle for the commercialization.[14]

In this context, recent works have suggested that quasi-2D structural MHPs exhibit enhanced stabilities to the surrounding stresses.[15–17] The quasi-2D MHPs show a basic structure of $(RNH_3)_2A_{n-1}M_nX_{3n+1}$ (<n> = 1, 2, 3, 4......).[18,19] Here, RNH$_3$, A, M, and X are the long-chain alkyl organic cations, the monovalent cation, the divalent metal cation, and the halide anion, respectively. The quasi-2D structure can be regarded as the mixture of 3D (based on the A cation) and 2D (based on the larger RNH$_3$ cation) structural MHPs.[20,21] In this structure, the large organic cation acts as potential barriers and the $(MX_6)^{4-}$

Y. Duan
State Key Laboratory of Organic Electronics and Information Displays &
Institute of Advanced Materials (IAM)
Nanjing University of Posts & Telecommunications
9 Wenyuan Road, Nanjing 210023, China

Y. Duan, X. Jin, D.-Y. Wang
IMDEA Materials Institute
Calle Eric Kandel, 2, 28906 Getafe, Spain

The ORCID identification number(s) for the author(s) of this article can be found under https://doi.org/10.1002/adfm.202209249.

F. E. Oropeza, V. A. de la Peña O'Shea
Photoactivated Processes Unit
IMDEA Energy Institute
Avda. Ramón de la Sagra, 3, Mostoles, 28935 Madrid, Spain

O. Amargós-Reyes, Y. Atoini, L. M. Cavinato, R. D. Costa
Chair of Biogenic Functional Materials
Technical University of Munich
Schulgasse 22, D-94315 XStraubing, Germany
E-mail: ruben.costa@tum.de

G. N. Nagy, M. U. Kahaly
ELI-ALPS, ELI-HU Non-Profit Ltd.
Wolfgang Sandner utca 3, H-6728 Szeged, Hungary

G. N. Nagy, M. U. Kahaly
Institute of Physics
University of Szeged
Dóm tér 9, H-6720 Szeged, Hungary

octahedral sheets sandwiched by two layers of large organic cations serve as potential wells. Therefore, the generated charge carriers can be spatially confined within the multiple-quantum-well structure, suppressing the exciton dissociation as well as improving the radiative recombination.[22,23] Thus, it comes as no surprise that quasi-2D MHPs have been largely applied to thin-film devices operating in an inert atmosphere.[15] However, their self-stability/working operation behaviors under ambient conditions have been scarcely investigated yet. This contrasts with the work focused on 3D MHPs in which the impact of the ambient stress is still controversial. For instance, early works showed that the photo-induced O_2^- species will cause the degradation of the $CH_3NH_3PbI_3$ layers,[24] while others determined that O_2 binds strongly to the surface iodide vacancy of $CH_3NH_3PbI_3$, leading to an efficient passivation on non-radiative defects,[25] achieving a long-term operational stability for the LEDs. In line with these lines, the use of quasi-2D MHPs as color filters for phosphor-converting LEDs (pc-LEDs) that operate under ambient conditions has been neglected. This is motivated by the fact that i) their PLQYs are much lower than those of 3D MHPs shielded by ligands or metal oxides and ii) the ambient stability of the quasi-2D MHPs has been typically considered as poor.

In this context, quasi-2D $(BA)_2(MA)_{n-1}Pb_nBr_{3n+1}$/PEO (BA, MA, and PEO are butylammonium $(CH_3(CH_2)_3NH_3^+)$, methylammonium $(CH_3NH_3^+)$, and polyethylene oxide, respectively) films were synthesized and investigated as the platform to explore the effect of the ambient stresses on their photoluminescence properties. The fresh films of $(BA)_2(MA)_3Pb_4Br_{13}$/PEO ($<n> = 4$ composition) show a high PLQY value of 55%, that surprisingly increases up to 74% upon storage under ambient conditions (no irradiation) after 100 days, while it strongly reduces under dark and inert atmosphere storage (38%). This is attributed to the passivation effect on surface Br vacancies by weakly adsorbed ambient water molecules as further confirmed by in situ/ex situ X-ray photoelectron spectroscopy (XPS). Furthermore, it is found that this passivation effect happens regardless of the introduced PEO. The passivation effects were also confirmed using Density-functional theory (DFT) simulations for $(BA)_2(MA)_3Pb_4Br_{13}$ films, showing that Br vacancies form on the films during the preparation process through a shallow boundary state and the preferential adsorption of H_2O onto the Br vacancy site will contribute to a more stable and favorable structure. This strongly encouraged us to prepare the quasi-2D MHPs based pc-LEDs, realizing maximal luminous efficiencies of 32 lm W^{-1} despite the ultrathin thickness ($\approx$60 nm), and stabilities of $\approx$400 h@10 mA. This represents a 20-fold enhanced device stability compared to those with analogous 3D-MAPbBr$_3$ filters (i.e., 23 h@10 mA and maximal luminous efficiencies of 15 lm W^{-1}), opening a new application path in the lighting field.

2. Results and Discussion

### 2.1. Preparation and Characterization of Quasi-2D Films

The quasi-2D $(BA)_2(MA)_{n-1}Pb_nBr_{3n+1}$/PEO composition thin-films were prepared through a one-step spin-coating process. Here, we first selected the $<n> = 3$ composition as the platform

to investigate the effect of PEO on the photoluminescence features of the films by blending different volume ratios of the $(BA)_2(MA)_2Pb_3Br_{10}$ precursor and PEO in Dimethylformamide (DMF).

Scanning electron microscopy (SEM) images (**Figure 1**) show the morphological evolution of the films upon increasing the concentration of PEO. In neat quasi-2D $(BA)_2(MA)_2Pb_3Br_{10}$ films (Figure 1a, no PEO), a large number of pinholes can be observed. The overall coverage of MHPs is very low ($\approx$70–80%). Smooth and pinhole free films were obtained after adding PEO. As shown in Figure 1b,c, less holes are noted as the PEO volume ratio increases, and the surface coverage can achieve to $\approx$90% for 20% ratio. Almost no big holes can be detected when the ratio is 33.33%, reaching a homogeneous layer at 42.86% PEO addition (Figure 1d,e). Here, the particle size gradually becomes smaller as the PEO ratio increases. This is also consistent with the previous work, in which 2,2′,2″-(1,3,5-Benzinetriyl)-tris(1-phenyl-1-H-benzimidazole) (TPBI) improves the morphology of the MAPbBr$_3$ via the crystal growth hindering.[26] This phenomenon was also observed by Shih's lab, who noted a significantly higher degree of surface coverage and smoothness in 2D FAPbBr$_3$-Poly(methyl methacrylate) (PMMA) films than those films without PMMA.[27]

As far as the photoluminescence features are concerned, a slightly blue shifted emission band and enhanced PLQY upon increasing the amount of PEO in the quasi-2D $(BA)_2(MA)_2Pb_3Br_{10}$/PEO films (Figure 1g,h) are noted, suggesting that the reduction of the particle size enhances the quantum confinement, leading to the improved photoluminescence behavior. Indeed, neat quasi-2D $(BA)_2(MA)_2Pb_3Br_{10}$ films show a PLQY of 10% that increases up to 26% in quasi-2D $(BA)_2(MA)_2Pb_3Br_{10}$/PEO-42.86 (42.86% volume ratio of PEO in the mixture solution) (Figure 1h; Table S1, Supporting Information). In addition, the quasi-2D $(BA)_2(MA)_2Pb_3Br_{10}$/PEO thin films show almost the same Ultraviolet-visible (UV–vis) absorption peaks and X-ray diffraction (XRD) patterns as the neat quasi-2D $(BA)_2(MA)_2Pb_3Br_{10}$, indicating that the introduction of PEO does not change MHPs' structure (Figures S1 and S2, Supporting Information). Beyond the optimized amount of PEO, big agglomerates evolved (Figure 1f), red shifting the emission peak and significantly decreasing the PLQY. Herein, low amount of PEO in the precursor solution can increase the viscosity and therefore contributes to the hindrance of the perovskite movement during the spin-coating process and then achieve highly continuous thin films.

Keeping in mind that the quasi-2D $(BA)_2(MA)_2Pb_3Br_{10}$/PEO-42.86 (42.86% PEO) films show the best optical properties and excellent morphologies, quasi-2D MHPs/PEO films (hereafter refers to the ones with the optimized amount of PEO) with different $<n>$ compositions were prepared through tuning the molar ratio of BABr:MABr:PbBr$_2$ in the precursor solution (Table S2, Supporting Information). As illustrated in **Figure 2**a, the $<n> = \infty$ is actually the extreme case of the layered $(BA)_2(MA)_{n-1}Pb_nBr_{3n+1}$, with a formula of MAPbBr$_3$. When the long chain BA molecule is introduced to the precursor solution, its radius is too big to insert into the corner-sharing 3D $(PbBr_6)^{4-}$ framework and thereby induces the 3D architecture to separate into layered MHPs with different n values.[22,28] Here, n represents the number of $(PbBr_6)^{4-}$ slab between two adjacent
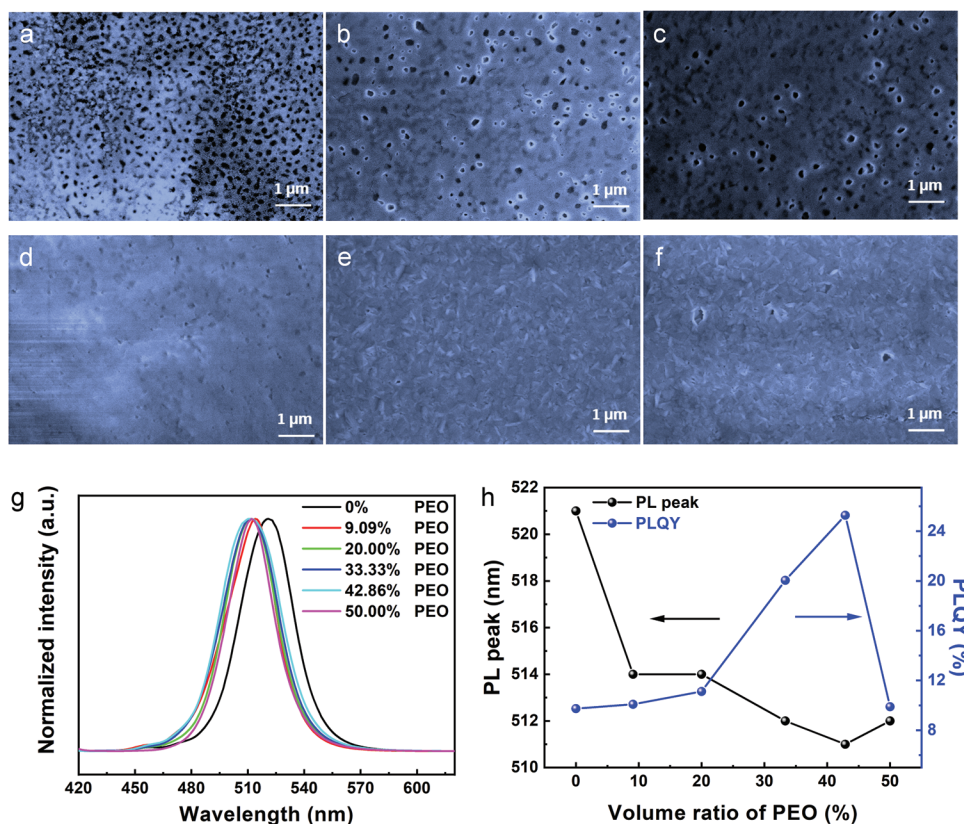
Figure 1. SEM images of a) neat quasi-2D $(BA)_2(MA)_2Pb_3Br_{10}$ thin film, and quasi-2D $(BA)_2(MA)_2Pb_3Br_{10}$/PEO thin films with PEO volume ratio of b) 9.09%, c) 20.00%, d) 33.33%, e) 42.86%, and f) 50.00%. Normalized emission spectra g) and maximum emission peaks associated with PLQY values h) of quasi-2D $(BA)_2(MA)_2Pb_3Br_{10}$/PEO composition thin films (see legend).

BA layers,[15] while symbol <n> represents the composition that was prepared based on the molar ratio of the introduced chemicals during the preparation (Table S2, Supporting Information). As reported before, the $(PbBr_6)^4$ slabs between large organic cations in the quasi-2D MHPs can behave as the quantum wells to confine the excitons and therefore improve the efficiency of the radiative recombination.[29]
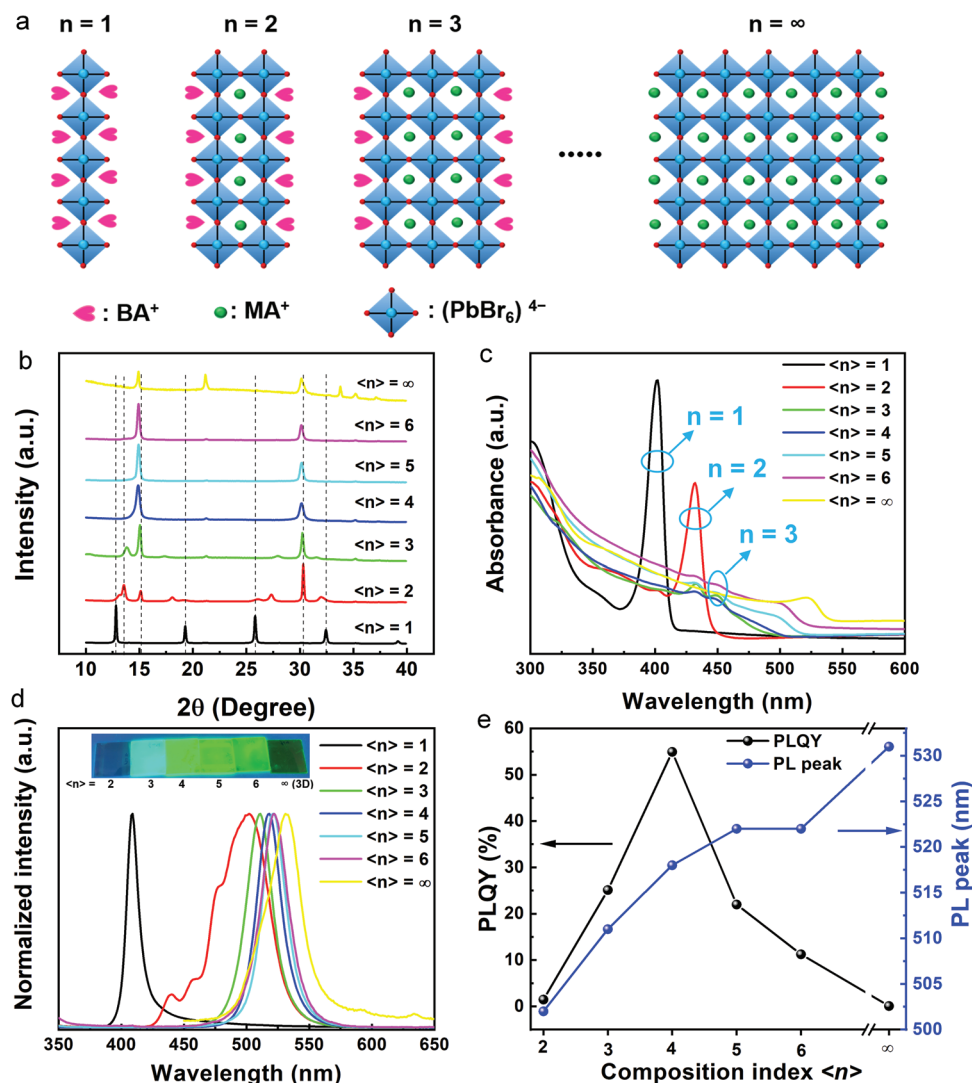
XRD measurements were conducted to determine the structural evolution of the MHPs (Figure 2b). All these quasi-2D MHPs/PEO films with <n> ≥ 2 compositions show strong diffraction peaks at ≈14.9° and 30.2° as well as weak peaks at 21.4° and 35.2° that are assigned to the (100), (110), (200), and (211) diffraction patterns of the 3D $MAPbBr_3$, respectively.[30,31] This also suggests that the quasi-2D MHPs are not a pure phase, but containing large n-phases (or 3D MHPs). Note that the full width at half maximum (FWHM) of these two strong diffraction peaks in the <n> = 4 films are much broader than in other compositions, indicating the generation of smaller crystals. In the case of <n> = ∞ films, a diffraction peak at 33.7° is also observed. This corresponds to the (210) plane of cubic $MAPbBr_3$ (space group: Pm3m).[30,31] In addition, diffraction patterns at angles lower than 14.8° are also observed due to the presence of quasi-2D MHPs grains.[32] The diffraction peaks located at 12.8°, 19.3°, 25.6°, 32.4° of <n> = 1 films are related to the n = 1 phase.[33] For the <n> = 2 films, new diffraction peaks located at 13.6°, 18.02°, 27.2° start to appear. Some diffraction patterns from the n = 2 phase can still be observed for <n> = 3

composition, but they are absent in the <n> ≥ 4 compositions. Finally, the shift in the diffraction peaks is caused by the incorporation of the large BA cations.

Next, the spectroscopic features (i.e., UV–vis absorption and emission spectra, PLQYs, excited-state lifetimes) were studied. The <n> = 1 (the 2D MHP) and <n> = ∞ compositions were considered for reference purposes. As shown in Figure 2c, additional absorption peaks at 402, 432, and 448 nm are observed after adding BA. They are assigned to the n = 1, 2, and 3 phases, respectively. In line with the XRD findings, only peaks belong to n = 1 phase are detected in the <n> = 1 composition, and both n = 1 and n = 2 phases are observed in the <n> = 2 composition. In addition, the n = 2 and 3 phases are observed in all the quasi-2D MHPs/PEO thin films, and the intensity becomes weaker as the <n> composition number increases. The peaks located at 498–521 nm of the <n> ≥ 4 compositions are from the MHPs that have n ≥ 4 phases, and these peaks show a red shift as the <n> composition number increases, suggesting that the band gap decreases as the thickness (n) of the inorganic $(PbBr_6)^{4-}$ slab increases.[34] Please note that only one peak at 521 nm appears in <n> = ∞ films, which is the characteristic absorption peak of the 3D $MAPbBr_3$.[35]

The emission features of the quasi-2D MHPs/PEO thin films are displayed in Figure 2d. The <n> = 1 (2D MHP/PEO) thin-films show a sharp emission peak at 409 nm (3.03 eV) with a long tail due to the self-trapped exciton emission.[33,36,37] All the quasi-2D MHPs/PEO thin films exhibit multiple emission

ADVANCED
SCIENCE NEWS
www.advancedsciencenews.com

ADVANCED
FUNCTIONAL
MATERIALS
www.afm-journal.de

Figure 2. a) The schematic illustration of the $(BA)_2(MA)_{n-1}Pb_nBr_{3n+1}$ structures; b) XRD patterns and c) UV–vis absorption spectra of $(BA)_2(MA)_{n-1}Pb_nBr_{3n+1}$/PEO thin films; d) Normalized PL spectra of the obtained $(BA)_2(MA)_{n-1}Pb_nBr_{3n+1}$/PEO thin films, inset is a photograph of the films with $<n>$ is 2, 3, 4, 5, 6, and ∞ under the 302 nm UV irradiation; e) PLQY and maximum emission peak evolution of the $(BA)_2(MA)_{n-1}Pb_nBr_{3n+1}$/PEO ($<n>$ is 2, 3, 4, 5, 6, and ∞) composition thin films.

bands (Figure S3, Supporting Information), which was also observed in the former work for the $PEA_2(FAPbBr_3)_{n-1}PbBr_4$.[20] These results are in line with the XRD and the UV–vis findings.

The 3D $MAPbBr_3$/PEO ($<n> = ∞$) thin films exhibit a distinct emission at 531 nm (2.34 eV). In addition, the emission band peaks of the quasi-2D MHPs/PEO films show a gradual blue shift and an increasing PLQY (Figure 2e; Table S3, Supporting Information). It is found that the $<n> = 4$ films show the highest PLQY and brightest green emission (Figure 2e and the inset in Figure 2d). This is also consitant with the morphological measurements from Atomic force microscopy (AFM) that the $<n> = 4$ films demonstrate the lowest roughness (Figure S5, Supporting Information). Then, the PLQY gradually declines as $<n>$ changes from 4 to 2 (1.48% at $<n> = 2$). Compared with the 3D $MAPbBr_3$/PEO ($<n> = ∞$) thin film, the significant improvement in the PLQY for the quasi-2D MHPs/PEO films is caused by the formation of quantum wells in the

structures, leading to a cascade energy transfer from the low to the high n phase. This significantly facilitates the radiative recombination.[34] Indeed, this is confirmed by the excited-state lifetimes values, showing that the $<n> = 4$ films feature the slowest decay (36.63 ns; Figure S6 and Table S3, Supporting Information).

In general, $n = 2$ and 3D ($<n> = ∞$) phases will dramatically affect the radiative recombination rate.[20,38] Based on the XRD, UV–vis and PL results, the $<n> = 3$ composition exhibits $n = 2$ phase, while no $n = 2$ phase is observed in the $<n> = 4$ composition through XRD (may be caused by the low content) and emission techniques. Only a weak peak from $n = 2$ phase is detected in the UV–vis spectra of the $<n> = 4$ composition. Finally, high percent of 3D phase will exist in the higher $<n>$ compositions ($<n> \geq 5$). Thus, it is not surprising that the highest PLQY is met in $<n> = 4$ films and the properties of these films will be further investigated.
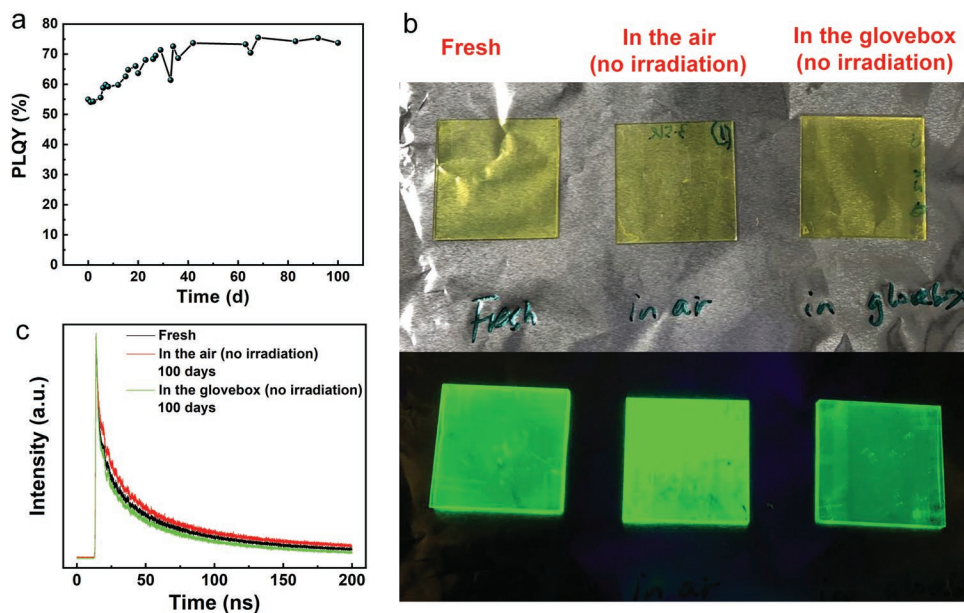
Figure 3. a) Changes of the PLQY over time for $(BA)_2(MA)_3Pb_4Br_{13}$/PEO ($<n> = 4$) films upon storage in the air (no irradiation); b) Photographs of fresh films, films stored in the air and glovebox (no irradiation) under day light (up) and UV light (down); c) The comparison of the emission decay curves for these films. All the measurements were done in Madrid, Spain. The temperature of the lab is kept at ≈25 °C all over the year, the average relative humidity of Madrid is ≈35% during our measurement.

2.2. Self-Stability upon Ambient Storage

As a next step, $(BA)_2(MA)_3Pb_4Br_{13}$/PEO films ($<n> = 4$) were stored in the air and glovebox (no irradiation) to investigate the effect of the ambient stresses on their properties. As shown in **Figure 3**a, the PLQY of the films stored in the dark air increases over the first 40 days going from ≈55% to 75% and holding at this value over extra 60 days (**Table 1**). However, the films kept in the glovebox (no irradiation) show a reduction in the PLQY value, down to 38% after 100 days (Table 1). This can also be seen by the photographs (Figure 3b), in which those stored in the dark air show brighter emission than the fresh films and those stored under inert and dry atmosphere (in the glovebox, no irradiation). In addition, the PLQY values (≈0.07%) of 3D MAPbBr$_3$/PEO ($<n> = \infty$) thin films show fluctuations after the same storage period, to 0.64% (in the dark air) and 0.35% (in the glovebox, without irradiation), but are still lower than 1%. We are not sure that this kind of fluctuations in the PLQY are attributed to the photo-brightening effect or the unavoidable errors during the measurement. Therefore, we could not make a clear conclusion for the 3D perovskite films currently, and we will focus on the investigation of these quasi-2D $<n> = 4$ films.

Further confirmation of the photo-brightening of the films stored under ambient (dark condition) came upon analyzing the excited-state lifetimes. As shown in Figure 3c, the films stored in the dark air (39 ns) show slower decays than the fresh films (36.6 ns), while those stored in the glovebox without irradiation show the fastest decay (34.8 ns), indicating exciton quenching due to the reduced surface trapping states. Finally, the radiative recombination rate (k_{rad}) and the nonradiative recombination rate (k_{nonrad}) were calculated using the following equations:[39,40]

$$\tau_{avg} = \frac{1}{k_{nonrad} + k_{rad}} \tag{1}$$

$$PLQY = \frac{k_{rad}}{k_{rad} + k_{nonrad}} \tag{2}$$

As a result, the k_{rad} shows the same increasing trend as PLQYs and the average excited-state lifetimes, whereas the k_{nonrad} shows the opposite trend (Table 1). Therefore, these results indicate that species in air, like moisture and oxygen, will increase the radiative recombination and then part of the traps in the films are passivated at the same time.

2.3. Origin of the Photo-Brightening Mechanism

To further confirm this statement, XRD and SEM were performed to investigate whether changes in the crystal structure

Table 1. PLQY, average excited-state lifetime, k_{rad}, and k_{nonrad} of the fresh and aged films stored in air and glovebox for 100 days.

Film	PLQY [%]	Average excited-state lifetimes [ns]	k_{rad} [×10⁻³ ns⁻¹]	k_{nonrad} [×10⁻³ ns⁻¹]
Fresh	54.73	36.62	15.0	12.3
In the air (no irradiation) for 100 days	73.73	39.00	18.9	6.7
In inert atmosphere (no irradiation) for 100 days	37.67	34.76	10.8	17.9
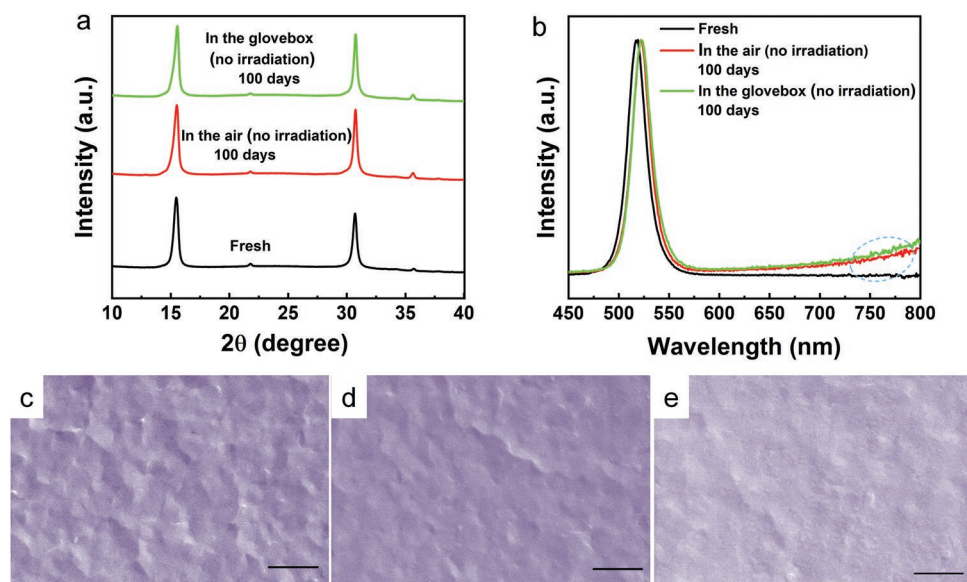
Figure 4. Comparison of the XRD patterns a) and emission spectra b) of fresh and aged films stored in the air and glovebox (no irradiation) after 100 days. SEM images of the fresh films c), the films stored in the glovebox (no irradiation) d) and air (no irradiation) e) after 100 days. The scale bar here is 1 μm.

and/or the surface of these quasi-2D/PEO films occur upon storage. As shown in **Figure 4**, XRD peaks and SEM images are identical for all these 3 films and no new peaks evolved, indicating that structures keep stable in both dark air and glovebox.
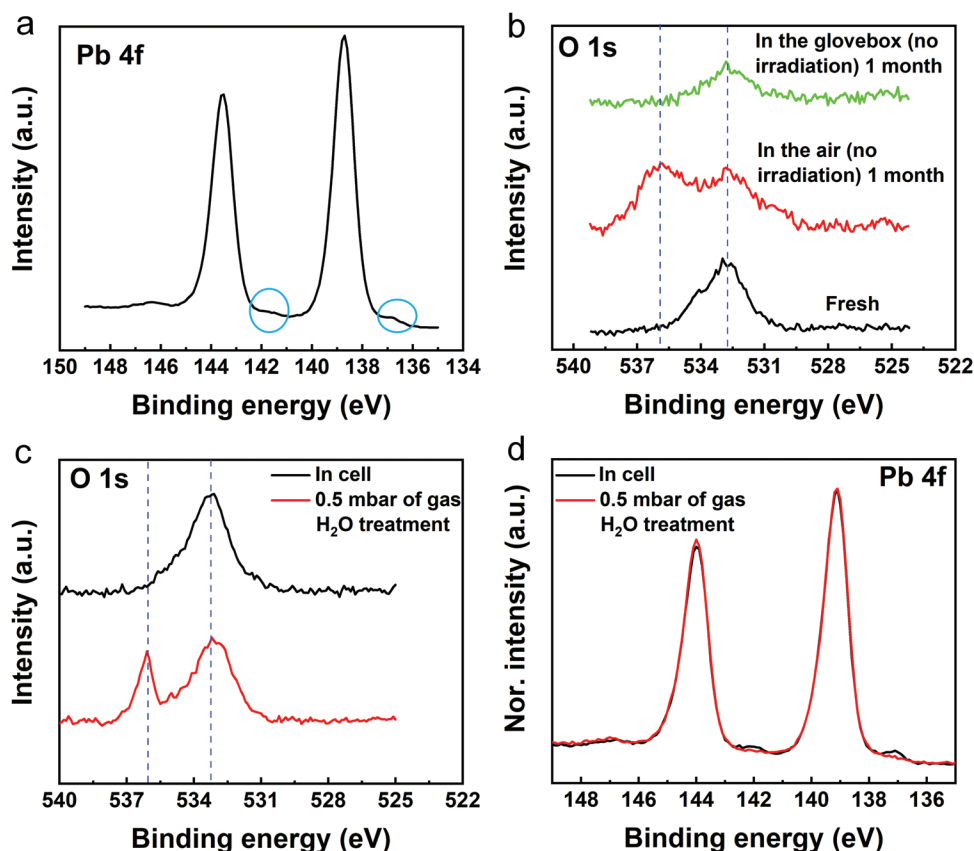
As reported previously, the defects in MHPs include shallow level trap states (SLTS) and deep level trap states (DLTS).[41,42] Herein, the SLTS mainly come from the point defects, like vacancies and interstitials, while the DLTS usually origin from the grain boundaries. They can be differentiated upon close inspection of the emission features (Figure 4b). A red shift of ≈3 nm is detected for both the films stored in the air and glovebox (no irradiation), suggesting slightly aggregation forms during this period, while a new emission band in the near infrared region evolves (Figure 4b; Figure S7, Supporting Information). This has been typically ascribed to the DLTS emission.[43] The presence of DLTS usually causes a strong reduction in the PLQYs that could explain the emission quenching noted in films stored in the glovebox, but it cannot explain the increased PLQY for films stored in the air. Thus, the photo-brightening under ambient storage must not be ascribed to the passivation effect of DLTS. Therefore, the passivation effect of the SLTS, like vacancies, should be responsible for the photo-brightening process. Actually, several works have shown that oxygen and water molecules can modulate the optical properties of MHPs. For instance, the increased PLQY of the $MAPbBr_3$ is attributed to the effect that water molecules passivate the Br-vacancy defects.[40] Other works have shown that the photoinduced superoxide (O_2^-) can bind with the halide vacancies, leading to the enhanced photoluminescence in I-based MHPs.[44,45] Here, the films were stored under dark condition, to exclude the formation of the O_2^-, leaving the surrounding moisture that is dynamically physisorbed (adsorption and desorption) passivating the surface trap without affecting the structure.

In addition, we also observed the PLQY evolution of the $(BA)_2(MA)_3Pb_4Br_{13}/PEO$ ($\langle n \rangle$ = 4) films stored in the air and irradiation (daily light). The PLQY shows an increase at the beginning to ≈71% in the first 5 days and then a gradual decrease (Figure S8, Supporting Information), which is different with the films stored in the dark air (Figure 3a). For the first 5 days, the enhanced PLQY is mainly attributed to the passivation effect from the water molecules. Then the continuously permeated O_2^- species (not exist in the films stored in the dark air) may react with the $\langle n \rangle$ = 4 films and cause their degradation, and therefore the fast decay. Meanwhile, the light-induced degradation and/or aggregation will also cause the decreased PLQY.

On the other hand, measurements on the $(BA)_2(MA)_3Pb_4Br_{13}$ films (no PEO) also shows photo-brightening for the first 8 days (Figure S9, Supporting Information) upon storage in the dark air, indicating that the water passivation effect happens regardless of PEO. However, the PLQY of these films show an obvious decrease even some fluctuations after the peak value, suggesting that PEO can help to improve the stability of these quasi-2D films. Therefore, PEO contributes to the initial PLQY of the films as well as the excellent stability upon storage, but not the water passivation effect.

X-ray photoelectron spectroscopy (XPS) analysis was further performed to prove our hypothesis about the passivation effect of the water molecules. Quantitative surface chemical analysis based on the photoelectron spectra shows that the Br/Pb ratio is below stoichiometric nominal value of the structure formula (Table S4, Supporting Information), suggesting that Br vacancies exist on the surface of the films. As shown in **Figure 5**a, the spectrum in the Pb 4f region of freshly prepared films shows the expected spin orbit doublet feature due to Pb (II) together with a low-binding-energy shoulder, which can be assigned to the metallic Pb (Pb^0). Such metallic Pb species can act as the quenching center and cause the decreased PLQY for films stored in the glovebox.[26] Meanwhile, a new peak at ≈535.8 eV in the O 1s region appears for films stored in the

**ADVANCED
SCIENCE NEWS**

www.advancedsciencenews.com

**ADVANCED
FUNCTIONAL
MATERIALS**

www.afm-journal.de

Figure 5. a) Pb 4f XPS spectra of the freshly prepared $<n>$ = 4 films. b) Comparison of the O 1s XPS spectra for the fresh films, the films stored in the air and glovebox (no irradiation) for 1 month. The comparison of c) O 1s XPS and d) Pb 4f spectra for the films upon in situ exposure of H_2O vapor. Herein, "in cell" refers to the films stored in the dark air for one month and then dried in the Ultra High Vacuum (UHV) for another month.
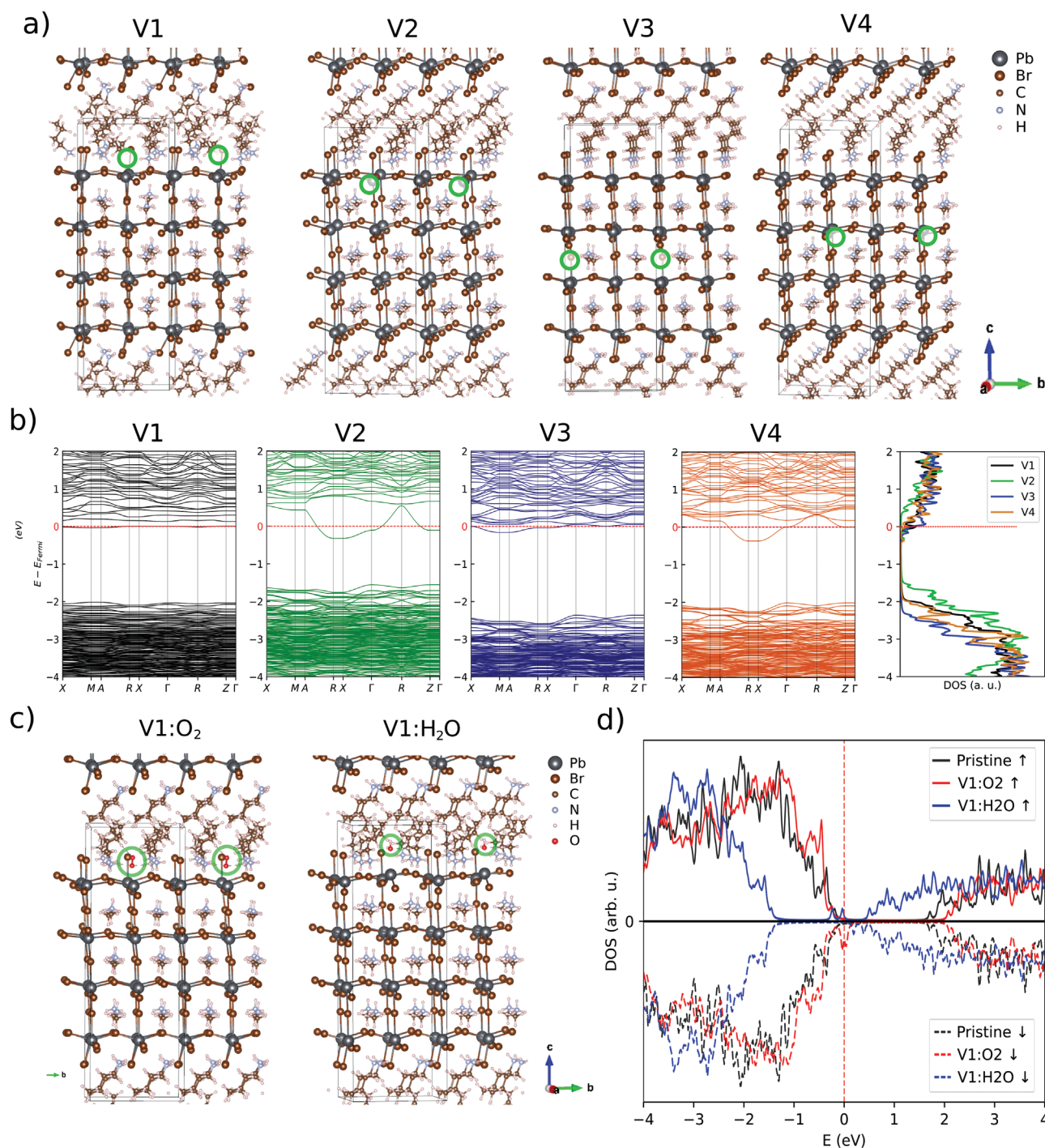
dark air for 1 month, which may be assigned to the adsorbed H_2O molecules (Figure 5b). However, this peak is not shown in the freshly prepared films and the films stored in the glovebox (no irradiation) for the same period, where only O 1s peak associated with the PEO capping can be observed. We believe that such H_2O surface species adsorbed from the air can passivate the Br vacancies. As shown in the XRD results in Figure 4a, the structure of these films did not degrade during the storage, suggesting that these H_2O molecules are physically/weakly adsorbed on Br vacancies.

Next, these films were stored under UHV for another month to observe the surface change. As expected, the O 1s peak at $\approx$535.8 eV disappears (Figure 5c), which indicates that these H_2O molecules are weakly adsorbed to the surface other than going inside the structure. Therefore, we conclude that the dynamic adsorption/desorption of the H_2O molecules contributes to the passivation effect on the Br vacancies that formed during the preparation process. Furthermore, an in situ experiment was conducted to investigate the effect of the continuous water treatment on these vacancies. During the experiment, 0.5 mbar of H_2O vapor was introduced to films via a leak valve, results were recorded after at least 15 min of pressure stabilization. An interesting observation is that, the spectral feature associated with metallic Pb peaks disappears accompanied by the appearance of the O 1s peak $\approx$535.8 eV under H_2O vapor (Figure 5c,d; Figures S10 and S11, Supporting Information),

indicating that H_2O molecules can indeed passivate the Br vacancies through removing the Pb^0 species. Particularly, our results prove a similar assumption as the former work that the introduction of water molecules results in the reduction of luminescence quenching site and therefore the enhanced PLQYs for the $MAPbBr_3$.[40,46,47] However, the insight is totally different with the previous work that the moisture-assisted surface passivation of $MAPbBr_3$ emitters is attributed to the oxidation of metallic Pb atoms and therefore the decreased numbers of surface defects.[46]

To explore the formation possibility and preferred location of Br vacancy within the perovskite crystal, DFT calculations were further carried out to estimate the Br vacancy formation energies and corresponding electronic structure of the perovskite films. We chose multiple Br vacancies, created at different surface and bulk sites, labeled as V1–V4 as shown in **Figure 6**a. Structure V1 corresponds to a single Br atom removed from the $MAPbBr_3$ layer boundary "embedded" into the BA molecular layer and can be considered as a shallow boundary vacancy. Structure V2 is obtained by creating a single Br vacancy at the Pb-Br layer of the $MAPbBr_3$ (001) surface close to the intercalated BA molecules and can be considered as a deep boundary vacancy (Figure 6a, V2). Within the deeper bulk-like $MAPbBr_3$ region, two vacancies at similar sites as to V1 and V2 were selected (V3 and V4 as shown in Figure 6a). The defect formation energy (**ΔEV**), corresponding to V1, V2, V3, and V4 states

**ADVANCED
SCIENCE NEWS**

www.advancedsciencenews.com

**ADVANCED
FUNCTIONAL
MATERIALS**

www.afm-journal.de

Figure 6. Perovskite films with Br vacancies at different locations: a) optimized structures with Br vacancy (locations shown with green circles) at the shallow boundary vacancy (V1), deep boundary vacancy (V2), bulk vacancy (V3), and deeper bulk vacancy (V4). b) Corresponding band structure and density of states (DOS) of these three systems with vacancies, plotted with respect to the Fermi level ($E_f = 0$, as shown by red dotted line). c) Optimized unit cell structures with O_2 and H_2O adsorbed into the V1 vacancy site. d) Comparison of the corresponding densities of states.

are obtained from the difference between the values for the pristine crystal and for the defective crystal (after removing single Br atom from chosen sites). From the trend of Br-vacancy formation energies **ΔEV**, as listed in **Table 2**, Br vacancies formation on the perovskite surface (V1 case) is energetically most favorable, followed by possible vacancy formation in the Pb-rich

layers close to the surface (V2 and V4) cases. Br defects thus should be detected within topmost few atomic surface layers of the MAPbBr$_3$ perovskite slabs.

Corresponding band structures for each Br vacancy case demonstrate a slight population of electronic states near the Fermi level, via a few bands from the lowest unoccupied states

**ADVANCED
SCIENCE NEWS**

www.advancedsciencenews.com

**ADVANCED
FUNCTIONAL
MATERIALS**

www.afm-journal.de

Table 2. Formation energies and the band gap or pseudo band gap (pseudo = *) of the pristine and V1-4 systems from the spin-restricted DFT calculations. For all perovskite structures with Br vacancies, conduction band minima cross the Fermi level, consequently, slight metallic states are present at the Fermi level, resulting in a pseudo bandgap.

	V1	V2	V3	V4
E_V (eV)	−1459.101	−1456.801	−1455.966	−1457.253
$E_V + E_{Br}$ (eV)	−1463.193	−1460.893	−1460.059	−1461.345
ΔE_V (eV)	−3.3275	−1.0276	−0.1925	−1.4793
$\Delta E_{pseudogap}$ (eV)	1.98(*)	1.23(*)	2.20(*)	1.64(*)

(Figure 6b). It should be noted that these band structures are the systems with vacancies and these vacancies introduce new lines in the bandgap. The band structure of the pristine system is shown in Figure S12 (Supporting Information). Thus Br-vacancy systems V1–V4 should rather be described as pseudogap systems (see the DOS in the right panel of Figure 6b). The pseudogaps ($\Delta E_{pseudogap}$) are listed in Table 2. Note that V2 and V4 scenarios correspond to similar vacancies in the Pb-rich (001) layer of the bulk perovskite, V2 is in the layer closest to the surface, while V4 locates one layer lower. We analyze that for each vacancy case, highly dispersive in-gap states originating from dangling bonds of Pb atoms occur within this major gap, which should indirectly contribute to the overall conductivities of the perovskites with Br vacancies.

To address the possible molecular adsorption onto the perovskite, we used different starting positions for the molecule X (X = O_2, H_2O) with respect to the Br vacancy site of the layered perovskite. The final relaxed structures and energetics suggest that H_2O or O_2 molecules can easily be physisorbed near the Br vacancy location, at the perovskite surface interfaced with BA layer (i.e., V1 case). H_2O molecule demonstrates obvious preferential binding, showing the positive adsorption energy of 2.09 eV (**Table 3**). Adsorption of H_2O is strongly favorable possibly as a means of compensation for the presence of Br vacancy. O_2 adsorption is energetically less favored (by ≈3.4 eV), however still feasible (Figure 6c). Our results thus indicate that the adsorption of H_2O onto the Br vacancy site (V1) of the layered perovskite $(BA)_2(MA)_3Pb_4Br_{13}$ is an exothermic process, releasing energy and thereby yielding a more stable and favorable structure. These trends strongly suggest the possibility of impressive stabilities of these perovskites under ambient storage. Interestingly, the adsorption of H_2O/O_2 molecules results in a prominent change in the electronic structures of the perovskites and leads to a sharp additional state near the Fermi level (Figure 6d). Two lone electron pairs from H_2O and O_2 molecules result in slight induced magnetic moments into the final structures V1:O_2 and V1:H_2O.

Table 3. Formation and adsorption energies of O_2 and H_2O into the V1 vacancy site, from spin-unrestricted calculations.

X	O_2	H_2O
E_{V1} (eV)	−1459.101	−1459.101
$E_{V1:X}$ (eV)	−1467.881	−1470.574
E_X (eV)	−7.441	−13.565
$\Delta E_{ads}^{V1:X}$ (eV)	−1.339	2.092

Therefore, these above results from the XPS and DFT provide 4 insights: i) Br vacancies form on the films during the preparation process through a shallow boundary state and, in turn, the photo-brightening in the quasi-2D films under ambient is attributed to the passivation effect of the H_2O molecules on the surface Br vacancies, ii) the adsorption of H_2O molecules onto the Br vacancy site is an exothermic process, releasing energy and thereby yielding a more stable and favorable structure, iii) the physically adsorbed H_2O molecules on the Br vacancies can be removed through exposing to the UHV for a long time, i.e., it is a reversible process, and iv) the presence of H_2O vapor reduces the amount of metallic Pb on the surface of the films, i.e., it causes a decrease in the concentration of surface Br vacancies, probably though a healing process.

2.4. Fabrication and Characterization of the pc-LEDs

To demonstrate the potential of the photo-brightening of quasi-2D MHP/PEO films, pc-LEDs devices were fabricated using the $<n> = 4$ films. In particular, films with the thickness of ≈60 nm were put above an LED chip emitting at 400 nm following a remote architecture and operating under ambient conditions upon increasing the applied current from 10 to 150 mA. For the devices fabricated with both $<n> = 4$ and $<n> = \infty$ films, the emission intensity enhances upon increasing applied currents (**Figure 7**a,b). Meanwhile, the devices fabricated with the $<n> = 4$ films show an enhanced luminous efficiency upon increasing currents that is prior to those with $<n> = \infty$ (3D MHP) filters (Figure S14, Supporting Information). Other characteristics of pc-LEDs devices are shown in Figure S15 (Supporting Information).

Stability measurements were carried out through driving the devices at 20 and 10 mA under ambient conditions. As expected, the $<n> = 4$ films-based devices show an excellent stability under both applied currents, reaching lifetimes of 203 and 384 h under 20 and 10 mA (Figure 7c,d), respectively. These devices demonstrate the most promising stability compared with other LEDs based on the quasi-2D perovskites (Table S6, Supporting Information). This sharply contrasts to the performances for the $<n> = \infty$ films (3D) based devices, in which the lifetimes are only 11 h (20 mA) and 23 h (10 mA) (Figure 7c,d). Particularly, the emission intensity increases quickly in the first hours for the $<n> = 4$ films. The superoxide forms under illumination, that is, the excited electrons of the MHPs react with the oxygen molecules after the physisorption process. The negatively charged O_2^- will bond with the positively charged Br vacancies (V_{Br}^+), leading to the improved emission.[44,48]
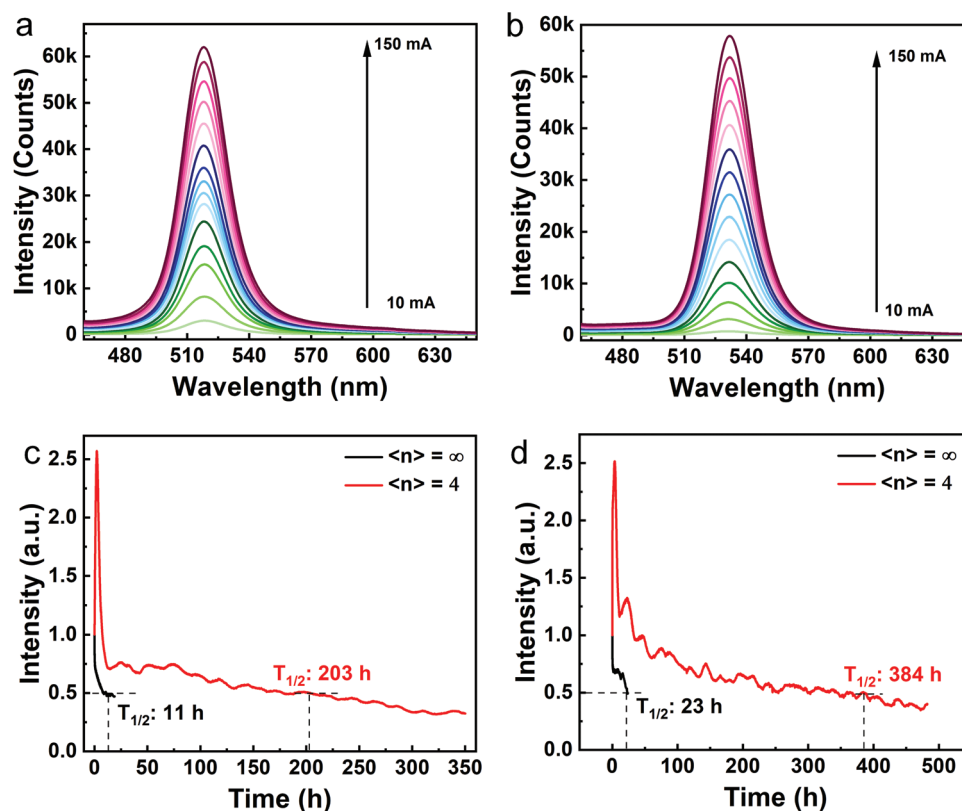
Figure 7. Emission spectra upon increasing applied currents for devices with a) $\langle n \rangle = 4$ films and b) $\langle n \rangle = \infty$ films. The operational stability of the pc-LEDs devices upon applying c) 20 and d) 10 mA. Herein, the values of counts do not represent the real intensity of the light, they are closely related with the integration time that set for the measurements.

Then the intensity of the emission presents a three-step decay, including a fast decay, a subsequent slow decay, and a plateau stage under both currents. As a comparison, the photostability of these films was also checked in the glovebox with the same applied current and distance as those in the air (Figure S16, Supporting Information). The devices demonstrate slightly higher and lower stability than ambient condition under 10 and 20 mA, respectively. However, the devices in the glovebox show continuous decay without the plateau stage. In the glovebox, the water-induced passivation effect and the generation of the O_2^- can be excluded. The gradually decreased intensity is mainly caused by the light-induced degradation and/or aggregation in the glovebox. Therefore, the continuously permeated O_2^- are the main species that cause the descending intensity in the air, they will react with the $\langle n \rangle = 4$ films and cause their degradation.[45] Meanwhile, the water passivation effect on the surface Br vacancies will compensate this negative effect and contribute to the excellent operational stability under ambient conditions.

condition (no irradiation), while those stored in inert/dry atmospheres show a reduced PLQY (38% after 100 days). The mechanism consists of a moisture passivation effect that repairs the SLTS defects in a dynamic adsorption and desorption process, as nicely confirmed by the in situ XPS measurement. DFT simulation results also confirmed that the adsorption of H_2O molecules onto the Br vacancy site can result in the passivation effect and yield a very stable and favorable structure, strongly supporting the expected stability of these perovskites under ambient storage. Capitalizing this unforeseen photo-brightening effect, we fabricated the first pc-LEDs with quasi-2D $(BA)_2(MA)_3Pb_4Br_{13}$/PEO films, realizing impressive stabilities of ≈ 400 h at 10 mA. This is ≈ 20 times higher stabilities than those of the reference devices with 3D-MHP/PEO filters (≈ 20 h at 10 mA). Hence, this work has provided the first and powerful experimental evidence to set in the prospect of Br-based quasi-2D MHPs for highly performing pc-LEDs operating in air thanks to their unique photo-brightening behavior.

3. Conclusion

This work provides the first study about self-stability under ambient conditions of uniform quasi-2D $(BA)_2(MA)_{n-1}Pb_nBr_{3n+1}$/PEO composition films. This is highlighted by a unique photo-brightening behavior that leads to an increase of the PLQY from 55% (fresh) to 74% after 100 days stored under ambient

4. Experimental Section

Materials: Lead (II) bromide (PbBr$_2$, 99.999%), Dimethylformamide (DMF, anhydrous), and Polyethylene oxide (PEO, average Mw $\approx 5\,000\,000$) were purchased from Sigma–Aldrich. Methylammonium bromide (MABr) and n-Butylammonium bromide (BABr) were obtained from Greatcell solar materials. All materials were used as received without further purification.

Films Preparation: The perovskite precursor was prepared through dissolving BABr, MABr, PbBr$_2$ in DMF, keeping the concentration of Pb^{2+} at 0.4 M. PEO was dissolved in DMF with a concentration of 10 mg mL^{-1} and then stirred at 60 °C for 1 h to get a homogenous solution before using. Then the perovskite precursor and PEO solution were mixed at a desired ratio and stirred at 60 °C overnight. The mixture was filtered using a filter (PTFE, 0.22 μm) before spin-coating. Then the above solution was spun-coated at 4,500 rpm for 60 s, followed by thermal annealing at 60 °C for 5 min. After that, quasi-2D (BA)$_2$(MA)$_{n-1}$Pb$_n$Br$_{3n+1}$/PEO compositions or neat quasi-2D (BA)$_2$(MA)$_{n-1}$Pb$_n$Br$_{3n+1}$ thin films with a thickness of ≈60 nm can be obtained. All these preparation processes were performed in an Ar-filled glovebox.

Characterization Techniques: UV–vis absorbance spectra were recorded through the spectrophotometer (UV-2600, SHIMADZU) using the absorption module. The emission spectra and the PLQYs of these films were measured by the FS5 spectrofluorometer with an SC-30 integrating sphere (EDINBURGH INSTRUMENTS). Field emission scanning electron microscopy (FESEM, FEI 600i, OXFORD INSTRUMENTS) was used to characterize the morphology of these films. X-ray powder diffraction (XRD, PANalytical) was conducted to investigate the crystal structures of these thin films using a CuKα as the X-ray source. X-ray photoelectron spectra (XPS) were recorded with a lab-based spectrometer (SPECS GmbH, Berlin) using monochromated Al Kα source (hν = 1486.6 eV, 50 W) as the excitation source. For the in situ measurement, water vapor dosing was carried out via a leak valve, NAP-XPS at all pressures were recorded after at least 15 min of pressure stabilization. The detailed information can be found in the Supporting Information. Atomic force microscopy (AFM) measurements were carried out with a Park XE150 instrument (Park Systems Corp., Suwon, South Korea), and the results were analyzed using the Gwyddion evaluation software.

Fabrication and Characterization of pc-LEDs: pc-LEDs were fabricated through putting the films above the UV-LED chip (400 nm) in a remote configuration. Keithley 2231A-30-3 triple channel DC and AvaSpec-2048L (Avantes, with a calibrated integrated sphere Avasphere 30-Irrad) were used to provide the current source and record the changes in the emission spectra, respectively.

DFT Methodology: The electronic structure and adsorption energy calculations reported here were carried out using DFT methodology implemented in ADF-BAND program.[49] The calculation of formation energies, adsorption energies, and electronic structures were obtained after a variable-cell energy minimization on the (BA)$_2$(MA)$_3$Pb$_4$Br$_{13}$ cell to obtain the bulk crystal vectors. A 2 × 2 × 1 supercell of the relaxed pristine lattice was used to create a Br vacancy, ensuring negligible interaction between the periodic images (imposed due to periodic boundary conditions for the simulation of periodic structures).[50] Convergence of the final energy after structural relaxation to within 3 mRy/atom was ensured for all calculations, which is proved to be enough for perovskite systems.[51]

To explore the Br vacancy stability and preferred location within the perovskite crystal, multiple Br vacancy locations, created at different surface and bulk sites, labeled as V1-V4 (see Figure 6), were chosen. A 3 × 3 × 1 k-point mesh was used to sample the irreducible Brillouin zone of the crystal, during geometry relaxation and next self-consistent field (SCF) calculations to obtain band structures and densities of states (DOS). Suitable pseudopotentials with Generalized Gradient Approximation (GGA) with Perdew–Burke–Ernzerhof (PBE) exchange correlation functional (GGA-PBE) were employed to incorporate both short- and long-range interactions. The formation energies of the vacancy defects were calculated as follows,

$$\Delta E_V = E_V + E_{Br} - E_{pr} \tag{3}$$

where E_{pr}, E_V, and E_{Br} are the relaxed energies of the pristine material, the material with the selected type of Br vacancy at the chosen site, and the isolated Br atom, respectively. Herein, $E_{pr} = -1459.866$ eV and $E_{Br} = -4.092$ eV. The vacancy formation energies are listed in Table 2.

Slab structures along (001) were used to adsorb the O$_2$ and H$_2$O molecules. The adsorption energy of X molecule ($\Delta E_{ads}^{V1:X}$), i.e., the binding energy of the adsorbed molecule to the adsorption site, was calculated as follows,

$$\Delta E_{ads}^{V1:X} = E_{V1:X} - (E_X + E_{V1}) \tag{4}$$

where X is either O$_2$ or H$_2$O, $\Delta E_{ads}^{V1:X}$ is the calculated formation energy of the system with adsorbed O$_2$/H$_2$O molecule. $E_{V1: X}$ is the relaxed energy of the molecular-passivated V1 vacancy, where molecule X = O$_2$ or H$_2$O. E_{V1} is the vacancy formation energy corresponding to V1 case (-1459.101 eV) and E_X is the formation energy of the isolated O$_2$/H$_2$O molecule. Based on this definition, a larger positive adsorption energy indicates a stronger attractive interaction between the adsorbed molecules and the surface of the pristine layered (BA)$_2$(MA)$_3$Pb$_4$Br$_{13}$ perovskite. All these adsorption energies are listed in Table 3.

Supporting Information

Supporting Information is available from the Wiley Online Library or from the author.

Acknowledgements

Conflict of Interest

The authors declare no conflict of interest.

Data Availability Statement

The data that support the findings of this study are available from the corresponding author upon reasonable request.

Keywords

**ADVANCED
SCIENCE NEWS**

www.advancedsciencenews.com

**ADVANCED
FUNCTIONAL
MATERIALS**

www.afm-journal.de

[1] M. Lu, J. Guo, S. Sun, P. Lu, J. Wu, Y. Wang, S. V. Kershaw, W. W. Yu, A. L. Rogach, Y. Zhang, *Nano Lett.* **2020**, *20*, 2829.

[2] L. Gao, L. N. Quan, F. P. García de Arquer, Y. Zhao, R. Munir, A. Proppe, R. Quintero-Bermudez, C. Zou, Z. Yang, M. I. Saidaminov, O. Voznyy, S. Kinge, Z. Lu, S. O. Kelley, A. Amassian, J. Tang, E. H. Sargent, *Nat. Photonics* **2020**, *14*, 227.

[3] E. S. Vasileiadou, B. Wang, I. Spanopoulos, I. Hadar, A. Navrotsky, M. G. Kanatzidis, *J. Am. Chem. Soc.* **2021**, *143*, 2523.

[4] Y. He, Y. Liang, S. Liang, Y. W. Harn, Z. Li, M. Zhang, D. Shen, Z. Li, Y. Yan, X. Pang, Z. Lin, *Angew. Chem., Int. Ed.* **2021**, *60*, 7259.

[5] H. Li, H. Lin, D. Ouyang, C. Yao, C. Li, J. Sun, Y. Song, Y. Wang, Y. Yan, Y. Wang, Q. Dong, W. C. H. Choy, *Adv. Mater.* **2021**, *33*, 2008820.

[6] Y. Duan, G. Z. Yin, D. Y. Wang, R. D. Costa, *ACS Appl. Mater. Interfaces* **2021**, *13*, 21800.

[7] Y. Duan, C. Ezquerro, E. Serrano, E. Lalinde, J. García-Martínez, J. R. Berenguer, R. D. Costa, *Adv. Funct. Mater.* **2020**, *30*, 2005401.

[8] H. Tsai, S. Shrestha, R. A. Vilá, W. Huang, C. Liu, C.-H. Hou, H.-H. Huang, X. Wen, M. Li, G. Wiederrecht, Y. Cui, M. Cotlet, X. Zhang, X. Ma, W. Nie, *Nat. Photonics* **2021**, *15*, 843.

[9] Y. Hassan, J. H. Park, M. L. Crawford, A. Sadhanala, J. Lee, J. C. Sadighian, E. Mosconi, R. Shivanna, E. Radicchi, M. Jeong, C. Yang, H. Choi, S. H. Park, M. H. Song, F. De Angelis, C. Y. Wong, R. H. Friend, B. R. Lee, H. J. Snaith, *Nature* **2021**, *591*, 72.

[10] Z. Chu, Y. Zhao, F. Ma, C. X. Zhang, H. Deng, F. Gao, Q. Ye, J. Meng, Z. Yin, X. Zhang, J. You, *Nat. Commun.* **2020**, *11*, 4165.

[11] C. Sun, Y. Zhang, C. Ruan, C. Yin, X. Wang, Y. Wang, W. W. Yu, *Adv. Mater.* **2016**, *28*, 10088.

[12] H. C. Wang, S. Y. Lin, A. C. Tang, B. P. Singh, H. C. Tong, C. Y. Chen, Y. C. Lee, T. L. Tsai, R. S. Liu, *Angew. Chem., Int. Ed.* **2016**, *55*, 7924.

[13] Z. K. Tan, R. S. Moghaddam, M. L. Lai, P. Docampo, R. Higler, F. Deschler, M. Price, A. Sadhanala, L. M. Pazos, D. Credgington, F. Hanusch, T. Bein, H. J. Snaith, R. H. Friend, *Nat. Nanotechnol.* **2014**, *9*, 687.

[14] Y. Duan, D. Y. Wang, R. D. Costa, *Adv. Funct. Mater.* **2021**, *31*, 2104634.

[15] L. Cheng, T. Jiang, Y. Cao, C. Yi, N. Wang, W. Huang, J. Wang, *Adv. Mater.* **2020**, *32*, 1904163.

[16] I. C. Smith, E. T. Hoke, D. Solis-Ibarra, M. D. McGehee, H. I. Karunadasa, *Angew. Chem., Int. Ed.* **2014**, *53*, 11232.

[17] H. Tsai, W. Nie, J. C. Blancon, C. C. Stoumpos, R. Asadpour, B. Harutyunyan, A. J. Neukirch, R. Verduzco, J. J. Crochet, J. Tretiak, L. Pedesseau, J. Even, M. A. Alam, G. Gupta, J. Lou, P. M. Ajayan, M. J. Bedzyk, M. G. Kanatzidis, *Nature* **2016**, *536*, 312.

[18] D. Zhang, Y. Fu, C. Liu, C. Zhao, X. Gao, J. Zhang, W. Guo, J. Liu, C. Qin, L. Wang, *Adv. Funct. Mater.* **2021**, *31*, 2103890.

[19] N. Yantara, A. Bruno, A. Iqbal, N. F. Jamaludin, C. Soci, S. Mhaisalkar, N. Mathews, *Adv. Mater.* **2018**, *30*, 1800818.

[20] X. Yang, X. Zhang, J. Deng, Z. Chu, Q. Jiang, J. Meng, P. Wang, L. Zhang, Z. Yin, J. You, *Nat. Commun.* **2018**, *9*, 570.

[21] J. Byun, H. Cho, C. Wolf, M. Jang, A. Sadhanala, R. H. Friend, H. Yang, T. W. Lee, *Adv. Mater.* **2016**, *28*, 7515.

[22] Z. Wang, F. Wang, W. Sun, R. Ni, S. Hu, J. Liu, B. Zhang, A. Alsaed, T. Hayat, Z. A. Tan, *Adv. Funct. Mater.* **2018**, *28*, 1804187.

[23] G. Xing, B. Wu, X. Wu, M. Li, B. Du, Q. Wei, J. Guo, E. K. Yeow, T. C. Sum, W. Huang, *Nat. Commun.* **2017**, *8*, 14558.

[24] N. Aristidou, I. Sanchez-Molina, T. Chotchuangchutchaval, M. Brown, L. Martinez, T. Rath, S. A. Haque, *Angew. Chem., Int. Ed.* **2015**, *127*, 8326.

[25] R. Brenes, C. Eames, V. Bulovic, M. S. Islam, S. D. Stranks, *Adv. Mater.* **2018**, *30*, 1706208.

[26] H. Cho, S.-H. Jeong, M.-H. Park, Y.-H. Kim, C. Wolf, C.-L. Lee, J. H. Heo, A. Sadhanala, N. Myoung, S. Yoo, *Science* **2015**, *350*, 1222.

[27] S. Kumar, J. Jagielski, N. Kallikounis, Y. H. Kim, C. Wolf, F. Jenny, T. Tian, C. J. Hofer, Y. C. Chiu, W. J. Stark, T. W. Lee, C. J. Shih, *Nano Lett.* **2017**, *17*, 5277.

[28] Y. Chen, Y. Sun, J. Peng, J. Tang, K. Zheng, Z. Liang, *Adv. Mater.* **2018**, *30*, 1703487.

[29] W. Deng, X. Jin, Y. Lv, X. Zhang, X. Zhang, J. Jie, *Adv. Funct. Mater.* **2019**, *29*, 1903861.

[30] M. H. Park, J. Park, J. Lee, H. S. So, H. Kim, S. H. Jeong, T. H. Han, C. Wolf, H. Lee, S. Yoo, T. W. Lee, *Adv. Funct. Mater.* **2019**, *29*, 1902017.

[31] Q. Zhou, Z. Bai, W. G. Lu, Y. Wang, B. Zou, H. Zhong, *Adv. Mater.* **2016**, *28*, 9163.

[32] Z. Xiao, R. A. Kerner, L. Zhao, N. L. Tran, K. M. Lee, T.-W. Koh, G. D. Scholes, B. P. Rand, *Nat. Photonics* **2017**, *11*, 108.

[33] L. Dou, A. B. Wong, Y. Yu, M. Lai, N. Kornienko, S. W. Eaton, A. Fu, C. G. Bischak, J. Ma, T. Ding, *Science* **2015**, *349*, 1518.

[34] N. Wang, L. Cheng, R. Ge, S. Zhang, Y. Miao, W. Zou, C. Yi, Y. Sun, Y. Cao, R. Yang, Y. Wei, Q. Guo, Y. Ke, M. Yu, Y. Jin, Y. Liu, Q. Ding, D. Di, L. Yang, G. Xing, H. Tian, C. Jin, F. Gao, R. H. Friend, J. Wang, W. Huang, *Nat. Photonics* **2016**, *10*, 699.

[35] H. Han, B. Jeong, T. H. Park, W. Cha, S. M. Cho, Y. Kim, H. H. Kim, D. Kim, D. Y. Ryu, W. K. Choi, C. Park, *Adv. Funct. Mater.* **2019**, *29*, 1808193.

[36] X. Wu, M. T. Trinh, D. Niesner, H. Zhu, Z. Norman, J. S. Owen, O. Yaffe, B. J. Kudisch, X. Y. Zhu, *J. Am. Chem. Soc.* **2015**, *137*, 2089.

[37] Z. Zhang, W.-H. Fang, M. V. Tokina, R. Long, O. V. Prezhdo, *Nano Lett.* **2018**, *18*, 2459.

[38] H. D. Lee, H. Kim, H. Cho, W. Cha, Y. Hong, Y. H. Kim, A. Sadhanala, V. Venugopalan, J. S. Kim, J. W. Choi, C. L. Lee, D. Kim, H. Yang, R. H. Friend, T. W. Lee, *Adv. Funct. Mater.* **2019**, *29*, 1901225.

[39] Y. J. Yoon, Y. Chang, S. Zhang, M. Zhang, S. Pan, Y. He, C. H. Lin, S. Yu, Y. Chen, Z. Wang, Y. Ding, J. Jung, N. Thadhani, V. V. Tsukruk, Z. Kang, Z. Lin, *Adv. Mater.* **2019**, *31*, 1901602.

[40] J. Jang, Y. H. Kim, S. Park, D. Yoo, H. Cho, J. Jang, H. B. Jeong, H. Lee, J. M. Yuk, C. B. Park, D. Y. Jeon, Y. H. Kim, B. S. Bae, T. W. Lee, *Adv. Mater.* **2021**, *33*, 2005255.

[41] Z. Ni, C. Bao, Y. Liu, Q. Jiang, W.-Q. Wu, S. Chen, X. Dai, B. Chen, B. Hartweg, Z. Yu, *Science* **2020**, *367*, 1352.

[42] T. A. S. Doherty, A. J. Winchester, S. Macpherson, D. N. Johnstone, V. Pareek, E. M. Tennyson, S. Kosar, F. U. Kosasih, M. Anaya, M. Abdi-Jalebi, Z. Andaji-Garmaroudi, E. L. Wong, J. Madeo, Y. H. Chiang, J. S. Park, Y. K. Jung, C. E. Petoukhoff, G. Divitini, M. K. L. Man, C. Ducati, A. Walsh, P. A. Midgley, K. M. Dani, S. D. Stranks, *Nature* **2020**, *580*, 360.

[43] R. Li, B. Li, X. Fang, D. Wang, Y. Shi, X. Liu, R. Chen, Z. Wei, *Adv. Mater.* **2021**, *33*, 2100466.

[44] P. Teng, S. Reichert, W. Xu, S.-C. Yang, F. Fu, Y. Zou, C. Yin, C. Bao, M. Karlsson, X. Liu, J. Qin, T. Yu, W. Tress, Y. Yang, B. Sun, C. Deibel, F. Gao, *Matter* **2021**, *4*, 3710.

[45] Y. Ju, X. g. Wu, S. Huang, G. Dai, T. Song, H. Zhong, *Adv. Funct. Mater.* **2021**, *32*, 2108296.

[46] H. Zhou, J. Park, Y. Lee, J. M. Park, J. H. Kim, J. S. Kim, H. D. Lee, S. H. Jo, X. Cai, L. Li, X. Sheng, H. J. Yun, J. W. Park, J. Y. Sun, T. W. Lee, *Adv. Mater.* **2020**, *32*, 2001989.

[47] J. M. Park, J. Park, Y. H. Kim, H. Zhou, Y. Lee, S. H. Jo, J. Ma, T. W. Lee, J. Y. Sun, *Nat. Commun.* **2020**, *11*, 4638.

[48] C. Zhao, C. Chen, X. Qiao, L. Luan, K. Lu, B. Hu, *Adv. Energy Mater.* **2015**, *5*, 1500279.

[49] G. te Velde, F. M. Bickelhaupt, E. J. Baerends, C. Fonseca Guerra, S. J. A. van Gisbergen, J. G. Snijders, T. Ziegler, *J. Comput. Chem.* **2001**, *22*, 931.

[50] H. Zhao, K. Chordiya, P. Leukkunen, A. Popov, M. Upadhyay Kahaly, K. Kordas, S. Ojala, *Nano Res.* **2021**, *14*, 1116.

[51] S. Nazir, M. Upadhyay Kahaly, U. Schwingenschlögl, *Appl. Phys. Lett.* **2012**, *100*, 201607.